Precision Electron-Beam Polarimetry at 1 GeV Using Diamond Microstrip Detectors

A. Narayan,[1] D. Jones,[2] J. C. Cornejo,[3] M. M. Dalton,[2,4] W. Deconinck,[3] D. Dutta,[1,*] D. Gaskell,[4] J. W. Martin,[5] K. D. Paschke,[2] V. Tvaskis,[5,6] A. Asaturyan,[7] J. Benesch,[4] G. Cates,[2] B. S. Cavness,[8] L. A. Dillon-Townes,[4] G. Hays,[4] E. Ihloff,[9] R. Jones,[10] P. M. King,[11] S. Kowalski,[12] L. Kurchaninov,[13] L. Lee,[13] A. McCreary,[14] M. McDonald,[5] A. Micherdzinska,[5] A. Mkrtchyan,[7] H. Mkrtchyan,[7] V. Nelyubin,[2] S. Page,[6] W. D. Ramsay,[13] P. Solvignon,[4] D. Storey,[5] A. Tobias,[2] E. Urban,[15] C. Vidal,[9] B. Waidyawansa,[11] P. Wang,[6] and S. Zhamkotchyan[7]

[1]*Mississippi State University, Mississippi State, Mississippi 39762, USA*
[2]*University of Virginia, Charlottesville, Virginia 22904, USA*
[3]*College of William and Mary, Williamsburg, Virginia 23187, USA*
[4]*Thomas Jefferson National Accelerator Facility, Newport News, Virginia 23606, USA*
[5]*University of Winnipeg, Winnipeg, Manitoba R3B 2E9, Canada*
[6]*University of Manitoba, Winnipeg, Manitoba R3T 2N2, Canada*
[7]*Yerevan Physics Institute, Yerevan, 375036, Armenia*
[8]*Angelo State University, San Angelo, Texas 76903, USA*
[9]*MIT Bates Linear Accelerator Center, Middleton, Massachusetts 01949, USA*
[10]*University of Connecticut, Storrs, Connecticut 06269, USA*
[11]*Ohio University, Athens, Ohio 45701, USA*
[12]*Massachusetts Institute of Technology, Cambridge, Massachusetts 02139, USA*
[13]*TRIUMF, Vancouver, British Columbia V6T 2A3, Canada*
[14]*University of Pittsburgh, Pittsburgh, Pennsylvania 15260, USA*
[15]*Hendrix College, Conway, Arkansas 72032, USA*

(Received 23 July 2015; revised manuscript received 18 November 2015; published 16 February 2016)

We report on the highest precision yet achieved in the measurement of the polarization of a low-energy, $\mathcal{O}(1\ \mathrm{GeV})$, continuous-wave (CW) electron beam, accomplished using a new polarimeter based on electron-photon scattering, in Hall C at Jefferson Lab. A number of technical innovations were necessary, including a novel method for precise control of the laser polarization in a cavity and a novel diamond microstrip detector that was able to capture most of the spectrum of scattered electrons. The data analysis technique exploited track finding, the high granularity of the detector, and its large acceptance. The polarization of the 180-μA, 1.16-GeV electron beam was measured with a statistical precision of $< 1\%$ per hour and a systematic uncertainty of 0.59%. This exceeds the level of precision required by the Q_{weak} experiment, a measurement of the weak vector charge of the proton. Proposed future low-energy experiments require polarization uncertainty $< 0.4\%$, and this result represents an important demonstration of that possibility. This measurement is the first use of diamond detectors for particle tracking in an experiment. It demonstrates the stable operation of a diamond-based tracking detector in a high radiation environment, for two years.

DOI: 10.1103/PhysRevX.6.011013 Subject Areas: Nuclear Physics, Particles and Fields

I. INTRODUCTION

High-precision physics experiments using polarized electron beams rely on accurate knowledge of beam polarization to achieve their ever-improving precision. A parity-violating electron-scattering experiment in Hall C at Jefferson Lab (JLab), known as the Q_{weak} experiment, is the most recent example [1,2]. The Q_{weak} experiment aims to test the Standard Model of particle physics by providing a first precision measurement of the weak vector charge of the proton, from which the weak mixing angle will be extracted with the highest precision away from the Z^0 pole. With the Q_{weak} experiment proposed to obtain a statistical precision of 2.1% on the parity-violating asymmetry, the uncertainty goal for beam polarimetry was 1%. Two future precision Standard Model tests at JLab, SOLID and MOLLER, have far more stringent polarimetry requirements of 0.4% [3,4].

In order to meet the high-precision requirement of the Q_{weak} experiment, a new polarimeter based on electron-photon scattering (Compton scattering) was constructed in experimental Hall C [2,5]. This polarimeter could be operated without disrupting the electron beam, allowing for

*Corresponding author.
d.dutta@msstate.edu

continuous polarization measurement during the Q_{weak} experiment. An existing polarimeter in Hall C, using a magnetized iron foil target to measure polarized e^-e^- scattering (Møller scattering) has previously reported a polarization measurement significantly better than 1% [6,7]. However, the Møller measurement is destructive to the polarized beam and requires reduced beam current; therefore, the results must be extrapolated in beam current and interpolated in time between the dedicated measurements.

In this paper, we present the first measurement of electron-beam polarization with the new Hall C Compton polarimeter, with the best precision ever achieved in this energy range (0.6%), and we directly compare the result with the Hall C Møller polarimeter. With each polarimeter reporting precision better than 1%, a direct comparison of the two independent measurements provides a valuable cross-check of electron-beam polarimetry techniques. These results also suggest that the rigorous demands of future experiments can be met.

Compton polarimetry is an established technique [8–18] which involves measuring a known QED double-spin asymmetry in electron scattering from a photon beam of known polarization. The scattering asymmetry varies with the fraction of electron-beam energy transferred to the scattered photon, with the maximum asymmetry occurring at the kinematic limit for maximum backscattered photon energy. The Compton-scattered electrons and photons can be independently measured and analyzed to determine the polarization of the electron beam. Most Compton polarization measurements have primarily analyzed the backscattered photons [8–16], and reliance on electron measurements has been less common [17,18]. Both the maximum scattering asymmetry and the maximum fraction of beam energy transferred to the photon increase quadratically with beam energy. For this reason, Compton-scattering measurements are significantly more difficult at low beam energies.

The SLC Large Detector (SLD) Compton polarimeter at the Stanford Linear Collider (SLC) [17] detected scattered electrons in a segmented gas Čerenkov detector with a reported precision of 0.5%—the only Compton polarimetry measurement more precise than this work. Operating at lower energies, the Compton polarimeter in Hall A at Jefferson Lab has reported a precision of about 1% by detecting the Compton-scattered electrons in a silicon microstrip detector [18] at a beam energy of 3 GeV and, in separate measurements, by integrating the total power of Compton-scattered photons in a total-absorption Gadolinium oxyorthosilicate (GSO) calorimeter [19] at 1–3 GeV [16,20].

The Q_{weak} measurement presented new challenges to this established polarimetry technology. The very precise SLD result was achieved with a 532-nm laser at a beam energy of 46.5 GeV, providing a maximum asymmetry $A_{\text{exp}} \sim 0.75$ and a maximum photon energy of almost 60% of the electron-beam energy. At the relatively low energy (1.16 GeV) of the electron beam for the Q_{weak} experiment, the maximum Compton asymmetry $A_{\text{exp}} \sim 0.04$ is significantly smaller, and only 5% of the electron energy can be transferred to the photon. The small asymmetry requires large luminosity to achieve sufficient statistical precision, while the lower kinematic limit implies that an electron detector must be positioned close to the primary beam and have high granularity to achieve suitable resolution on the scattered electron momentum.

The electron accelerator at Jefferson Lab operates at 1497 MHz with a beam repetition rate of 499 MHz to each of the three experimental halls and a bunch width of ≈0.5 ps. The small 2-ns spacing between each beam bunch implies that from the perspective of most detectors, the electron beam is essentially CW. In Compton polarimeters used in colliders (for example at the Hadron Electron Ring Accelerator (HERA) and SLD), the repetition rate of the electron beam was quite modest (on the order of 100 s of Hz), and it was possible to use low average power, pulsed lasers to achieve high instantaneous scattering rates, and hence excellent background suppression. This approach was not possible at Jefferson Lab, and a CW laser system was required.

The desired high luminosity was achieved by storing laser photons in a Fabry-Pérot cavity, even though past measurements of the laser polarization have proven to be challenging in evacuated Fabry-Pérot cavities. An innovative technique for maximizing the laser polarization by analyzing the reflected light at the cavity entrance was employed during the Q_{weak} experiment.

The high signal count rate, expected large background close to the beam, and proposed experimental run of 200 days required the selection of radiation-hard detection systems. A diamond microstrip detector was selected for electron detection. The well-established radiation hardness of diamond [21,22] and its insensitivity to synchrotron radiation were the most important considerations in this choice. While diamond microstrip detectors have been demonstrated in test beams [23,24], and other diamond detector configurations have been used in beam condition monitors [25–30], this is the first application of a diamond detector in an experiment as a particle tracking detector.

II. THE HALL C COMPTON POLARIMETER

A schematic of the Compton polarimeter in Hall C at JLab is shown in Fig. 1, and details can be found in Refs. [2,5]. The CW electron beam was deflected vertically by two dipole magnets to where it could interact with the photon target. Circularly polarized 532-nm laser light was injected into a Fabry-Pérot optical cavity, in the beam-line vacuum, with a gain of approximately 200. The injection laser, a Coherent Verdi [31] with an output of 10 W, was locked to the cavity. The 0.85-m long optical cavity crossed the electron beam at 1.3 °.

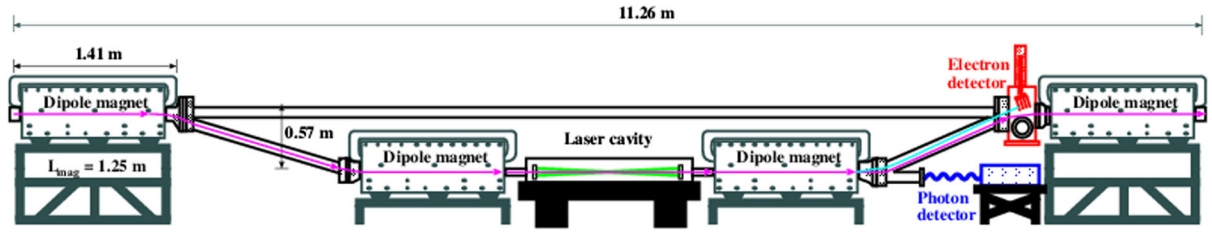

FIG. 1. Schematic diagram of the JLab Hall C Compton polarimeter. Four identical dipole magnets form a magnetic chicane that displaces the 1.16-GeV electron beam vertically downward by 0.57 m. An external low-gain Fabry-Pérot laser cavity provides a high-intensity (about 1.7 kW) beam of circularly polarized green (532-nm) photons. The laser light is focused at the interaction region ($\sigma_{\text{waist}} \sim 90\ \mu$m), and it is larger than the electron-beam envelope ($\sigma_{x/y} \sim 40\ \mu$m). The photon detector was not used for these results.

After interacting with the photon target, the electron beam was deflected back to the nominal beam line with a second pair of dipole magnets. The Compton-scattered photons passed through an aperture in the third magnet and were detected in an array of $PbWO_4$ crystals. The analysis of the detected photons was used as a cross-check of the electron analysis. The third chicane magnet bent the primary beam by 10.1°, also separating the Compton-scattered electrons from the primary beam by up to 17 mm before the fourth dipole. Here, the scattered electrons were incident on the electron detector, a set of four planes of diamond microstrip detectors. Remote actuation allowed the detector distance to the primary beam to be varied. Data were taken with the innermost strip a mere 5 mm from the beam, with routine operation at 7 mm from the beam. This range allowed the detection of most of the Compton electron spectrum, including the zero crossing of the asymmetry 8.5 mm from the primary beam.

The electron detectors were made from $21 \times 21 \times 0.5$ mm^3 plates of synthetic diamond grown using chemical vapor deposition (CVD) [32]. A novel Ti-Pt-Au metalization was used to deposit electrodes on the diamond plates. Each diamond plate has 96 horizontal metalized electrode strips with a pitch of 200 μm (180 μm of metal and a 20-μm gap) on one side. The Compton spectrum is spread over 50–60 strips, allowing a precise measurement of the shape. A schematic of a single detector plane is shown in Fig. 2. The strips were read out using custom low noise amplifiers and discriminators, grouped together with 48 channels in a single module [33]. The detector signal (about 9000 e^-) is transported to the readout electronics on a set of 55-cm long, 5-layer, Kapton flexible printed circuit boards [34] with a capacitance of 60–90 pF. The noise and gain for a typical channel was about 1000 e^- and 100 mV/fC, respectively. The low backgrounds resulting from the insensitivity of the diamond detectors to synchrotron radiation, together with the low noise of the readout, in spite of its large separation from the detectors, helped mitigate the challenges posed by the small signal size of diamond detectors.

The detectors were operated in single electron mode. The data acquisition (DAQ) system employed a set of field programmable gate array (FPGA) based logic modules [35] to implement a track-finding algorithm, which generated a trigger when a strip in the same cluster of four adjacent strips was identified in multiple active planes. The Compton-scattered electrons are approximately perpendicular to the detector planes and almost colinear with the incident electron beam; hence, they deviate by < 2 strips between the planes furthest apart. Three detector planes were used during the experiment, and the typical trigger condition required two out of three planes with a trigger rate of 70–90 kHz. The strip hits were histogrammed on the FPGA modules and read out during each helicity reversal (beam helicity was reversed at a rate of 960 Hz). Untriggered hits were also recorded and were used for studying DAQ dead time and trigger inefficiencies. With the track-finding trigger, electronic noise was suppressed by a factor of 100–200 compared to the untriggered mode, which led to a significantly better signal-to-background ratio in the triggered mode, but at the cost of a few percent DAQ inefficiency due to the combination of

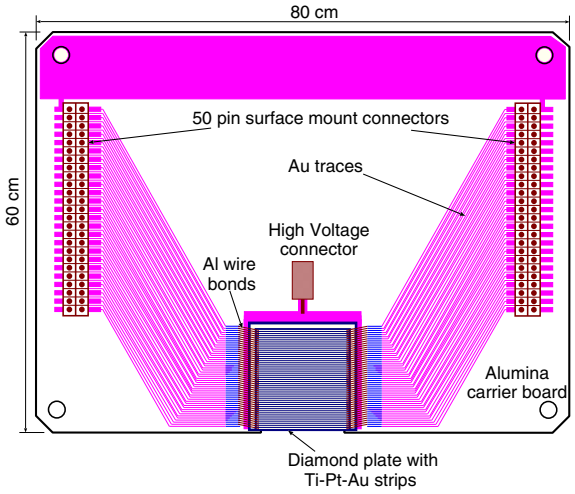

FIG. 2. A schematic diagram of the CVD diamond plate mounted on an alumina frame, which forms a single detector plane. There were 96 Ti-Pt-Au strips deposited on the front face of the diamond plate, which was attached to the frame using a silver epoxy. The strips were connected to Au traces on the alumina frame with aluminum wire bonds. The traces terminated on two 50-pin connectors. A high voltage (HV) bias of about −300 V was applied to the back side of the diamond plate via a miniature HV connector.

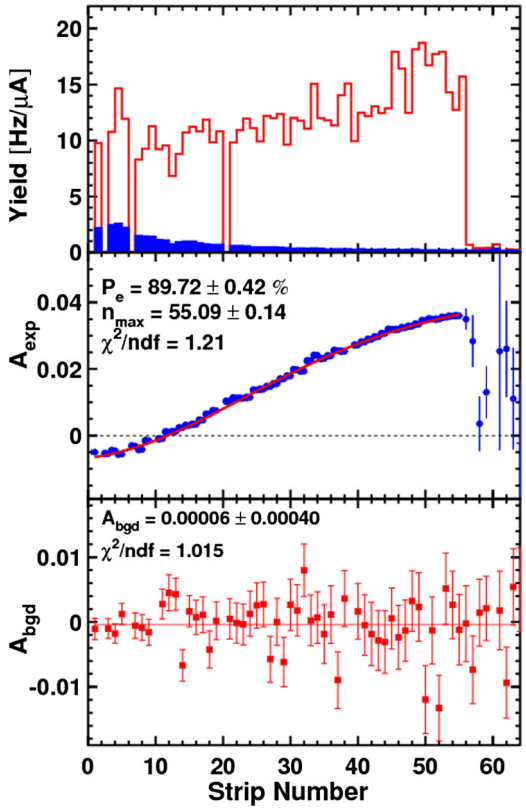

FIG. 3. Yield and asymmetry data from a single detector plane plotted versus detector strip number, for a typical hour-long run. Statistical uncertainties only. (Top panel) The charge normalized yield at a beam current of 180 μA and laser intensity of 1.7 kW. The laser-on yield is shown in red, and the laser-off (background) yield is shown in shaded blue. (Middle panel) The measured Compton asymmetry (background-subtracted). The solid red line is a fit to Eq. (2). (Bottom panel) The background asymmetry from the laser-off period. The solid red line is a fit to a constant value.

dead time and trigger inefficiency. Improvements in the DAQ design can readily eliminate these inefficiencies in the future. Although they were not needed for this application, the hits on all planes and the track information can be readily used to improve the resolution of the detector; however, a careful determination of the strip-wise efficiency for each plane would be required in order to determine the total detector efficiency.

For a beam current of 180 μA and a laser intensity of 1.7 kW, the total untriggered rate in the detector was 130–180 kHz (about 2.5 kHz per strip). The well-tuned electron-beam, low-noise electronics, and the insensitivity of diamond to synchrotron radiation contributed to a signal-to-background ratio of $\mathcal{O}(10)$, as demonstrated by the Compton and the background spectra shown in Fig. 3 (top panel). The detector efficiency was estimated to be 70% by comparing the expected to the observed rates. The small signal sizes, large distance between the detector and the readout electronics, and a threshold to reduce noise led to the inefficiency. Over the 2-year running period of the Q_{weak} experiment, the detectors were exposed to a radiation dose of 100 kGy from electrons (synchrotron radiation not included). No degradation of the detector performance was observed, demonstrating the intended radiation hardness and the stability of the charge collection process over extended periods, which is relevant for using diamond as tracking detectors. The strip-to-strip variation in efficiency, which was shown to have a negligible impact on the asymmetry measurement, may be of concern in other applications.

III. ANALYSIS AND RESULTS

The electron-beam helicity was reversed at a rate of 960 Hz in a pseudorandom sequence of quartets. The Compton laser was operated in 90-second cycles (60 s on and 30 s off). The laser-off data were used to measure the background, which was subtracted from the laser-on yield for each electron helicity state The signal-to-background ratio was 5–20, depending on the strip. The measured asymmetry was built from the yields using

$$A_{\text{exp}} = \frac{Y^+ - Y^-}{Y^+ + Y^-}, \tag{1}$$

where $Y^{\pm} = N^{\pm}_{\text{on}}/Q^{\pm}_{\text{on}} - N^{\pm}_{\text{off}}/Q^{\pm}_{\text{off}}$ is the charge normalized Compton yield for each detector strip, $N^{\pm}_{\text{on/off}}$ is the number of detected counts, and $Q^{\pm}_{\text{on/off}}$ is the beam charge, accumulated during the laser (on/off) period for the ($\pm$) electron helicity state. A statistical precision of $< 1\%$ per hour was routinely achieved. Typical yield spectra for the laser-on and laser-off periods are shown in Fig. 3 (top). Consistent results were obtained by subtracting the background over 1 laser cycle (90 s) and also over about 900 s. A typical spectrum for an hour-long run is shown in Fig. 3. The background asymmetry is consistent with zero within the statistical uncertainties.

The electron-beam polarization P_e was extracted by fitting the measured asymmetry to the theoretical Compton asymmetry, using

$$A^n_{\text{exp}} = P_e P_\gamma A^n_{\text{th}}, \tag{2}$$

where P_γ is the polarization of the photon beam and A^n_{th} is the $\mathcal{O}(\alpha)$ theoretical Compton asymmetry for fully polarized electrons and photon beams in the nth strip. The theoretical Compton asymmetry $A_{\text{th}}(\rho)$ was calculated as a function of the dimensionless variable

$$\rho = \frac{E_\gamma}{E^{\max}_\gamma} \approx \frac{E^{\text{beam}}_e - E_e}{E^{\text{beam}}_e - E^{\min}_e}, \tag{3}$$

where E_γ is the energy of a backscattered photon, $E^{\max}_\gamma$ is the maximum allowed photon energy, and E_e, $E^{\min}_e$, and E^{beam}_e are the scattered electron energy, its minimum value, and the electron-beam energy, respectively. A^n_{th} is related to

$A_{\mathrm{th}}(\rho)$ by mapping ρ to the strip number. The mapping is performed using the knowledge of the magnetic field in the third dipole, the geometry of the chicane, the strip pitch and the position of the kinematic end point (Compton edge) expressed as a strip position n_{max}. An initial estimate of the kinematic end point, n_{max}, was determined from the edge of the yield spectrum. It was observed to vary slowly, as the electron-beam angle drifted, by up to ± 0.5 mrad.

Radiative corrections to the Compton asymmetry were calculated to leading order with a low-energy approximation applicable for few-GeV electrons [36]. The radiative correction to the asymmetry was $< 0.3\%$ in all strips.

Equation (2) was fit to the measured asymmetries with P_e and n_{max} as the two free parameters. No systematic deviation of the shape of the asymmetry was observed. A typical fit is shown in Fig. 3. The χ^2 per degree of freedom of the fit, considering statistical uncertainties only, ranges between 0.8 and 1.5 for 50–60 degrees of freedom. The detection of a large fraction of the Compton electron spectrum, spanning both sides of the zero crossing of the Compton asymmetry, significantly improved the robustness of the fit. The fit quality was validated using the simulation discussed below.

The systematic uncertainty in the determination of P_e is summarized in Table I. In previous polarimeters using a laser system based on a Fabry-Pérot cavity, knowledge of the laser polarization was a significant source of uncertainty. Previous quoted uncertainties for the laser polarization have been larger than the total uncertainty for the present measurement. At Jefferson Lab, for example, uncertainties ranging from 0.6% to 1.1% have been reported [14–16].

TABLE I. Systematic uncertainties.

Source	Uncertainty	$\Delta P/P\%$
Laser polarization	0.18%	0.18
Helicity correl. beam	5 nm, 3 nrad	<0.07
Plane to plane	Secondaries	0.00
Magnetic field	0.0011 T	0.13
Beam energy	1 MeV	0.08
Detector z position	1 mm	0.03
Trigger multiplicity	1–3 planes	0.19
Trigger clustering	1–8 strips	0.01
Detector tilt (x, y and z)	1 degree	0.06
Detector efficiency	0.0–1.0	0.1
Detector noise	up to 20% of rate	0.1
Fringe field	100%	0.05
Radiative corrections	20%	0.05
DAQ efficiency correction	40%	0.3
DAQ efficiency pt.-to-pt.		0.3
Beam vert. pos. variation	0.5 mrad	0.2
Spin precession in chicane	20 mrad	<0.03
Electron detector total		0.56
Grand Total		0.59

Pressure induced birefringence in the vacuum window can lead to large changes in laser polarization that cannot be directly measured in the evacuated beam line. More recently, a precision of 0.3% [37] has been quoted for laser polarization in a Fabry-Pérot cavity; however, even in this case, the birefringence in the vacuum window was not measured directly. Our experience suggests that without direct measurements of the window birefringence, inferred knowledge of the laser polarization in the Fabry-Pérot cavity can be flawed. A technique that bypasses this requirement is needed.

Figure 4 shows our implementation of a scheme based on an optical reversibility theorem [38], which relates the polarization ellipticity at the output of an optical system to the polarization of the retro-reflected light at the input, in order to maximize the circular polarization in the cavity. The technique works by analyzing the light reflected from the entrance mirror of the cavity. A polarizing beam splitter (PBS), half-wave plate, and quarter-wave plate were used to create an arbitrary polarization state, which was then propagated to the cavity through an optical system with unknown birefringence, dominated by a vacuum window. Minimizing the polarization signal, the back-reflected light that is transmitted through the PBS maximizes the degree-of-circular-polarization (DOCP) at the cavity entrance mirror.

Representing the initial (linear) laser-polarization state after the PBS as $\boldsymbol{\varepsilon_1}$, the polarization vector at the first cavity mirror ($\boldsymbol{\varepsilon_2}$) is given by $\boldsymbol{\varepsilon_2} = M_E \boldsymbol{\varepsilon_1}$. Here, M_E represents the transport through all the optical elements to the cavity entrance mirror ($\lambda/2$, $\lambda/4$, and VW in Fig. 4). Assuming no polarization loss, transport backwards through the same

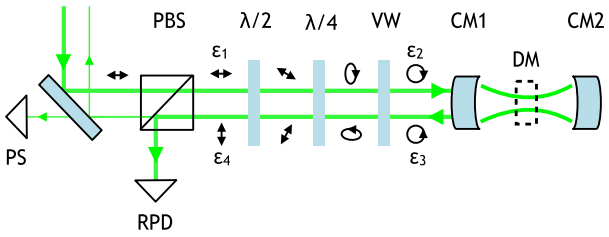

FIG. 4. Scheme for maximizing the circular polarization at the cavity. Laser light entering the system passes through a PBS, half-wave plate ($\lambda/2$), quarter-wave plate ($\lambda/4$), and vacuum window (VW) before it is either reflected off the cavity entrance mirror (CM1) or becomes resonant in the cavity. Note that in this figure, the element VW also includes three steering mirrors, which are incorporated in the model but left out of the figure for simplicity. Depending on the polarization state at CM1, reflected light will either arrive in a reflected photodiode (RPD), used for frequency-locking feedback, or be sampled by the polarization signal (PS) photodiode behind a steering mirror. Light arriving at the cavity entrance mirror is fully circular when there is no signal in PS. Before the experiment, with part of the beam-line vacuum pipe removed, it was possible to do a direct measurement (DM) of the circular polarization in the cavity.

optical system can be written as the transpose of the forward matrix, M_E^T. In the formalism of Ref. [38], the polarization vector does not change when the light direction changes, and the vector representing the light reflected from the cavity mirror (ε_3) is equivalent to ε_2. Therefore, the polarization of the light reflected from the cavity after transport backwards through the optical system is $\varepsilon_4 = M_E^T M_E \varepsilon_1$. The optical reversibility theorem dictates that for a linear polarization vector ε_1, the polarization at the cavity entrance (ε_2) is circular only if ε_4 is linear and orthogonal to ε_1. This means that the PBS, which creates the initial linear polarization state, will not allow the orthogonal reflected state to pass through; hence, minimization of the laser power propagating backwards through this cube ensures circular polarization at the cavity. Reference [37] used an implementation of the optical reversibility theorem that is equivalent to maximizing the signal in the RPD of Fig. 4. This is less sensitive than measuring polarization in extinction, such as minimizing the signal in the PS of Fig. 4, and was not used as their primary method.

To determine the uncertainty in the photon polarization, this DOCP maximization technique was directly tested *in situ*. With the vacuum enclosure removed, the intracavity DOCP was measured simultaneously with the polarization signal while scanning over input polarization states, with a concentration of points near the maximum DOCP, as in Fig. 5, demonstrating a very close and robust correlation. The uncertainty on the laser polarization is estimated to be 0.18%, which is dominated by our ability to bound, through direct measurement, effects that might alter the polarization over the numerous reflections within the Fabry-Pérot cavity. It is expected that this bound can be improved following methods implemented in Ref. [39], in particular, using an optical isolator to capture the full polarization signal. This would improve the signal-to-background ratio and allow us to study a locked cavity with arbitrary polarization (only near-circular polarization is possible with the current system). Effects of analyzing power, depolarization, or spatial polarization gradients are bound by the degree of extinction in the polarization signal and are included in the quoted laser-polarization uncertainty [40].

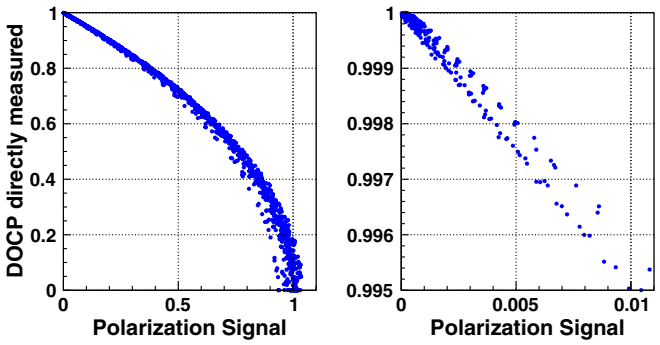

FIG. 5. Direct test of the laser-polarization maximization technique. The correlation between the laser DOCP directly measured after the cavity mirror and the polarization signal extracted from the reflected light. The left panel shows the full range, while the right panel is a zoomed-in version of the region of maximum DOCP.

The uncertainties in the measured asymmetry were studied using a Monte Carlo simulation of the Compton polarimeter, which was coded using the GEANT3 [41] detector simulation package. In addition to Compton scattering, the simulation included backgrounds from beam-gas interactions and beam-halo interactions in the chicane elements. It also incorporated the effects of detector efficiency, the track-finding trigger, and electronic noise. A typical simulated strip-hit spectrum (ideal, with noise, and with noise and efficiency) and the asymmetry extracted from it are shown in Fig. 6. The simulation was used to study the analysis procedure and the statistical quality of the fits that were used to extract the beam polarization. It was demonstrated that the central value of the polarization fit parameter was typically insensitive to small distortions to the electron spectrum such as a few missing or noisy strips and the observed strip-to-strip variation in efficiency. The simulation was also used to study a variety of sources of systematic uncertainties. For each source, the relevant parameter was varied within the expected range of uncertainty, and the range of variation of the extracted polarization was listed as its contribution to the systematic uncertainty.

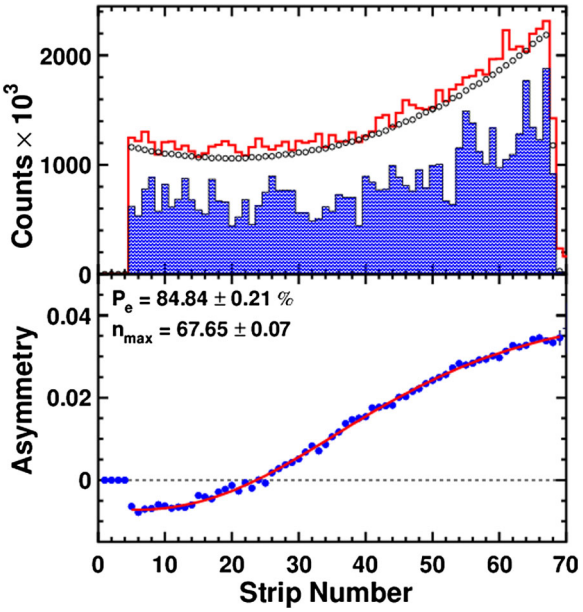

FIG. 6. (Top panel) Typical Monte Carlo simulated Compton spectra for a single detector plane; ideal (black open circles), with noise (red), and with detector efficiency (blue, shaded). (Bottom panel) The Compton asymmetry extracted from the simulated spectrum including detector efficiency (blue circles), and a two-parameter fit to the calculated asymmetry (red line). The input asymmetry was 85%.

The Monte Carlo simulation demonstrated that secondary particles knocked out by the Compton-scattered electron passing through the first detector plane produced a 0.4% change in the extracted polarization in the subsequent planes, consistent with observation. A correction for the second and third planes could be made but at the cost of a slightly higher systematic uncertainty, and hence, only the results from the first detector plane are quoted here. Although all three planes were used in the tracking trigger, the results from the first detector plane were shown by the simulation to be insensitive to this effect.

There were several sources of rate-dependent efficiency associated with the DAQ system, such as the algorithm used to identify electron tracks and form the trigger, and the dead time due to a busy (hold-off) period in the DAQ. A digital logic simulation platform, Modelsim [42], was used to model the DAQ system. Simulated Compton events, backgrounds, and noise signals were processed with this model, which made a detailed account of the logic and delays from the internal signal pathways in the FPGA modules and the external electronic chain.

These results were used to determine a correction to the detector yields, for each hour-long run, based on the detector rates during the run. This correction is calculated and applied for each beam helicity state independently. An estimate of the systematic uncertainty due to this correction was determined from the variation of the ratio of the polarizations extracted from the corrected, triggered data to those obtained from the untriggered data over a wide range of signal rates and several difference trigger conditions. The DAQ efficiency correction resulted in $< 1\%$ change in the extracted polarization.

The extracted beam polarization for the entire second running period of the Q_{weak} experiment is shown in Fig. 7. Changes at the electron source, indicated by the dashed and solid vertical lines, led to discontinuities in the beam polarization. Each point is shown with systematic uncertainties that may vary for each measurement, while a common systematic uncertainty of 0.42% applies to all points together.

These results are quantitatively compared to results [2] from the Møller polarimeter by examining periods of stable polarization between changes in the polarized source. Previous cross-comparisons between polarimeters in this energy range have uncovered significant discrepancies between various polarimeters [43]. The ratio of Compton to Møller measurements, when averaged over these stable periods using statistical and point-to-point systematic uncertainties, was 1.007 ± 0.003. The results are compatible within the total relative normalization uncertainty of 0.77%. This is the first direct comparison of two independent polarimeters with better than 1% precision.

Future experiments will require a polarimetry precision of 0.4% with beam energies between 6 and 11 GeV. Our results indicate that these goals are within reach of

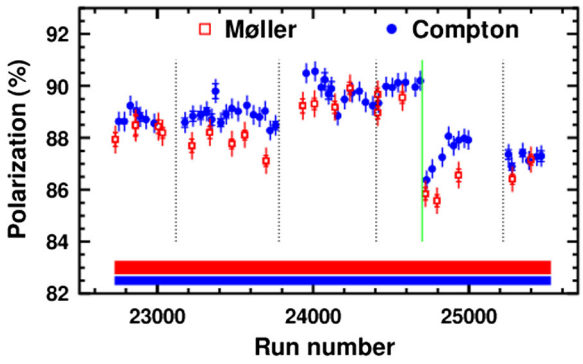

FIG. 7. The extracted beam polarization for the 1.16-GeV, 180-μA electron beam, as a function of run number and averaged over 30-hour-long periods, during the second-run period of the Q_{weak} experiment (blue, solid circle). Also shown are the results from the intermittent measurements with the Møller polarimeter [2] (red, open square). The inner error bars show the statistical uncertainty, while the outer error bar is the quadrature sum of the statistical and point-to-point systematic uncertainties. The solid bands show the additional normalization or scale-type systematic uncertainty (0.42% Compton and 0.65% Møller). The dashed and solid (green) vertical lines indicate changes at the electron source.

Compton polarimetry. Recent results using a photon detector in integrating mode [16] have demonstrated that uncertainties in the photon analysis (excluding the laser polarization) are at the level of 0.5%. Such a measurement could be combined with an independent electron analysis as demonstrated here, with a precision approaching 0.5%, with the dominant systematic error in common between the two analyses being the uncertainty on intracavity laser polarization ($< 0.2\%$). It is worth noting that further gains are possible: The dominant errors in the electron analysis relate to rate-dependent DAQ inefficiencies, which would undoubtedly be reduced through refinement of the logic and timing parameters, while improvements in gain stability and linearity measurements would further improve the photon measurements. The increased beam energies for planned future measurements are also more favorable to Compton polarimetry.

IV. CONCLUSIONS

The polarization of a 1.16-GeV CW electron beam was measured with a systematic uncertainty of 0.59%. The interacting photon polarization was maximized and the uncertainty reduced using a novel technique based on the reflected incident light. We used diamond microstrip detectors for the first time as tracking detectors and demonstrated their ability to withstand a high radiation dose, as well as their stability over long periods. The high granularity of the detectors and the measurement of a large fraction of the Compton electron spectrum, spanning the asymmetry zero crossing, coupled with a robust analysis technique and rigorous simulations of the polarimeter and

the DAQ system, produced a reliable, high-precision measurement of the polarization in a high-radiation environment. Because of these technical advances, the uncertainty goal was significantly surpassed. These results suggest that even more precise electron-beam polarization measurements, such as required for the future parity-violation measurements SOLID and MOLLER, will be achievable through Compton polarimetry. Furthermore, diamond-based tracking detectors are the superior choice for high-radiation environments and should find more widespread use.

ACKNOWLEDGMENTS

This work was funded by the U.S. Department of Energy, including Contract No. AC05-06OR23177 under which Jefferson Science Associates, LLC operates the Thomas Jefferson National Accelerator Facility, and by the U.S. National Science Foundation and the Natural Sciences and Engineering Research Council of Canada (NSERC). We wish to thank the staff of JLab, TRIUMF, and MIT-Bates for their vital support. We thank H. Kagan from Ohio State University for teaching us about diamonds, training us on characterizing them, and helping us build the prototype detector, and Tanja Horn and Ben Raydo at Jefferson Lab for suggesting and assisting with the FPGA-based readout scheme for the electron detector. We also acknowledge the University of Manitoba Nano Systems Fabrication Lab for the use of their facilities.

[1] D. Androic *et al.*, *First Determination of the Weak Charge of the Proton*, Phys. Rev. Lett. **111**, 141803 (2013).
[2] T. Allison *et al.*, *The* Q_{weak} *Experimental Apparatus*, Nucl. Instrum. Methods Phys. Res., Sect. A **781**, 105 (2015).
[3] MOLLER Collaboration, *The MOLLER Experiment: An Ultra-Precise Measurement of the Weak Mixing Angle Using Møller Scattering*, arXiv:1411.4088.
[4] P. Souder *et al.*, *Precision Measurement of Parity-Violation in Deep Inelastic Scattering Over a Broad Kinematic Range*, JLab Proposal No. PR12-10-007 (2012).
[5] A. Narayan, Ph.D. thesis, Mississippi State University, 2015 (unpublished).
[6] M. Hauger *et al.*, *A High-Precision Polarimeter*, Nucl. Instrum. Methods Phys. Res., Sect. A **462**, 382 (2001).
[7] J. Magee, *Sub-percent Precision Møller Polarimetry in Experimental Hall C*, *Proc. Sci.*, PSTP2013 (2013) 039.
[8] D. Gustavson, J. J. Murray, T. J. Phillips, R. F. Schwitters, C. K. Sinclair, J. R. Johnson, R. Prepost, and D. E. Wiser, *A Backscattered Laser Polarimeter* e^+e *Storage Rings*, Nucl. Instrum. Methods **165**, 177 (1979).
[9] L. Knudsen, J. P. Koutchouk, M. Placidi, R. Schmidt, M. Crozon, J. Badier, A. Blondel, and B. Dehning, *First Observation of Transverse Beam Polarization in LEP*, Phys. Lett. B **270**, 97 (1991).
[10] D. P. Barber *et al.*, *The HERA Polarimeter and the First Observation of Electron Spin Polarization at HERA*, Nucl. Instrum. Methods Phys. Res., Sect. A **329**, 79 (1993).
[11] I. Passchier, D. W. Higinbotham, C. W. de Jager, B. E. Norum, N. H. Papadakis, and N. P. Vodinas, *A Compton Backscattering Polarimeter for Measuring Longitudinal Electron Polarization*, Nucl. Instrum. Methods Phys. Res., Sect. A **414**, 446 (1998).
[12] M. Beckmann *et al.*, *The Longitudinal Polarimeter at HERA*, Nucl. Instrum. Methods Phys. Res., Sect. A **479**, 334 (2002).
[13] W. Franklin, *The MIT-Bates Compton Polarimeter*, AIP Conf. Proc. **675**, 1058 (2003).
[14] M. Baylac *et al.*, *First Electron Beam Polarization Measurements with a Compton Polarimeter at Jefferson Laboratory*, Phys. Lett. B **539**, 8 (2002); N. Felletto *et al.*, Nucl. Instrum. Methods Phys. Res., Sect. A **459**, 412 (2001).
[15] S. Escoffier *et al.*, *Accurate Measurement of the Electron Beam Polarization in JLab Hall A Using Compton Polarimetry*, Nucl. Instrum. Methods Phys. Res., Sect. A **551**, 563 (2005).
[16] M. Friend *et al.*, *Upgraded Photon Calorimeter with Integrating Readout for the Hall A Compton Polarimeter at Jefferson Lab*, Nucl. Instrum. Methods Phys. Res., Sect. A **676**, 96 (2012).
[17] K. Abe *et al.*, *High-Precision Measurement of the Left-Right Z Boson Cross-Section Asymmetry*, Phys. Rev. Lett. **84**, 5945 (2000); M. Woods, arXiv:hep-ex/9611005.
[18] A. Acha *et al.* (HAPPEX Collaboration), *Precision Measurements of the Nucleon Strange Form Factors at* Q^2 0.1 GeV^2, Phys. Rev. Lett. **98**, 032301 (2007).
[19] D. S. Parno, M. Friend, V. Mamyan, F. Benmokhtar, A. Camsonne, G. B. Franklin, K. Paschke, and B. Quinn, *Comparison of Modeled and Measured Performance of a GSO Crystal as Gamma Detector*, Nucl. Instrum. Methods Phys. Res., Sect. A **728**, 92 (2013).
[20] S. Abrahamyan *et al.*, *Measurement of the Neutron Radius of* ^{208}Pb *through Parity Violation in Electron Scattering*, Phys. Rev. Lett. **108**, 112502 (2012).
[21] C. Bauer *et al.*, *Radiation Hardness Studies of CVD Diamond Detectors*, Nucl. Instrum. Methods Phys. Res., Sect. A **367**, 207 (1995).
[22] M. M. Zoeller *et al.*, *Performance of CVD Diamond Microstrip Detectors under Particle Irradiation*, IEEE Trans. Nucl. Sci. **44**, 815 (1997).
[23] F. Borchelt *et al.*, *First Measurements with a Diamond Microstrip Detector*, Nucl. Instrum. Methods Phys. Res., Sect. A **354**, 318 (1995).
[24] R. J. Tapper, *Diamond Detectors in Particle Physics*, Rep. Prog. Phys. **63**, 1273 (2000).
[25] J. Bol, E. Berdermann, W. deBoer, E. Grigoriev, F. Hauler, and L. Jungermann, *Beam Monitors for TESLA Based on Diamond Strip Detectors*, IEEE Trans. Nucl. Sci. **51**, 2999 (2004).
[26] M. Bruinsma, P. Burchat, S. Curry, A. J. Edwards, H. Kagan, R. Kass, D. Kirkby, S. Majewski, and B. A. Petersen, *Radiation Monitoring with CVD Diamonds and PIN Diodes at BABAR*, Nucl. Instrum. Methods Phys. Res., Sect. A **583**, 162 (2007).

[27] P. Dong, R. Eusebi, C. Schrupp, A. Sfyrla, R. Tesarek, and R. Wallny, *Beam Condition Monitoring with Diamonds at CDF*, IEEE Trans. Nucl. Sci. **55**, 328 (2008).

[28] A. Bell *et al.*, *Fast Beam Conditions Monitor BCM1F for the CMS Experiment*, Nucl. Instrum. Methods Phys. Res., Sect. A **614**, 433 (2010).

[29] J. Pietraszko, L. Fabbietti, W. Koenig, and M. Weber, *Diamonds as Timing Detectors for Minimum-Ionizing Particles: The HADES Proton-Beam Monitor and START Signal Detectors for Time of Flight Measurements*, Nucl. Instrum. Methods Phys. Res., Sect. A **618**, 121 (2010).

[30] D. Dobos *et al.*, *Commissioning and First Operation of the pCVD Diamond ATLAS Beam Conditions Monitor*, Nucl. Instrum. Methods Phys. Res., Sect. A **623**, 405 (2010).

[31] *Operators Manual Verdi TM V-8/V-10 Diode-Pumped Lasers, Coherent, Inc. 08/2005*, Part No. 0174-929-00.

[32] The CERN grade diamond plates were procured from Element Six, New York, NY.

[33] Q_{weak} Amplifier Discriminator (QWAD), custom built by TRIUMF, Canada.

[34] Flexible printed circuit boards manufactured by Kadflx Inc., Nashua, NH.

[35] V1495 modules from CAEN Technologies, Inc., Staten Island, NY.

[36] A. Denner and S. Dittmaier, *Complete $\mathcal{O}(\alpha)$ QED Corrections to Polarized Compton Scattering*, Nucl. Phys. **B540**, 58 (1999).

[37] V. Brisson, R. Chiche, M. Jacquet, C. Pascaud, V. Soskov, Z. Zhang, F. Zomer, M. Beckingham, and N. Coppola, *Per Mill Level Control of the Circular Polarisation of the Laser Beam for a Fabry-Perot Cavity Polarimeter at HERA*, J. Instrum. **5**, P06006 (2010).

[38] N. Vansteenkiste, P. Vignolo, and A. Aspect, *Optical Reversibility Theorems for Polarization: Application to Remote Control of Polarization*, J. Opt. Soc. Am. A **10**, 2240 (1993).

[39] P. Asenbaum and M. Arndt, *Cavity Stabilization Using the Weak Intrinsic Birefringence of Dielectric Mirrors*, Opt. Lett. **36**, 3720 (2011).

[40] D. C. Jones, Ph.D. thesis, University of Virginia, 2015 (unpublished); arXiv:1601.07172.

[41] *CERN Program Library Long Write-up W5013*, 1993 (unpublished).

[42] *Modelsim Reference Manual, Mentor Graphics Corp.*, 2010 (unpublished).

[43] J. Grames *et al.*, *Unique Electron Polarimeter Analyzing Power Comparison and Precision Spin-Based Energy Measurement*, Phys. Rev. ST Accel. Beams **7**, 042802 (2004).